

# Realization of Rectangular Artificial Spin Ice and Direct Observation of High Energy Topology

I. R. B. Ribeiro,<sup>1,2</sup> F.S. Nascimento,<sup>3</sup> S.O. Ferreira,<sup>4</sup> W. A. Moura-Melo,<sup>4</sup> C. A. R. Costa,<sup>5</sup> J. Borme,<sup>6</sup> P. P. Freitas,<sup>6</sup> G. M. Wysin,<sup>7</sup> C.I.L. de Araujo,<sup>1,\*</sup> and A. R. Pereira<sup>4,†</sup>

<sup>1</sup>Laboratory of Spintronics and Nanomagnetism (LabSpiN), Departamento de Física, Universidade Federal de Viçosa, 36570-000 - Viçosa - Minas Gerais - Brazil.

<sup>2</sup>Instituto Federal do Espírito Santo, Alegre, 36570-900, Espírito Santo, 29520-000, Brazil

<sup>3</sup>Departamento de Física, Universidade Federal de Ouro Preto, 35931-008 - João Monlevade - Minas Gerais - Brazil.

<sup>4</sup>Departamento de Física, Universidade Federal de Viçosa, 36570-000 - Viçosa - Minas Gerais - Brazil.

<sup>5</sup>National Nanotechnology Laboratory (LNNano), National Center for Energy and Materials (CNPEM), Campinas, São Paulo, Brazil 13083-970

<sup>6</sup>INL-International Iberian Nanotechnology Laboratory, 4715-330, Braga, Portugal

<sup>7</sup>Department of Physics, Kansas State University, Manhattan, KS 66506-2601

(Dated: December 1, 2021)

In this letter, we have constructed and experimentally investigated frustrated arrays of dipoles forming two-dimensional artificial spin ices with different lattice parameters (rectangular arrays with horizontal and vertical lattice spacings denoted by  $a$  and  $b$  respectively). Arrays with three different ratios  $\gamma = a/b = \sqrt{2}$ ,  $\sqrt{3}$  and  $\sqrt{4}$  are studied. Theoretical calculations of low-energy demagnetized configurations for these same parameters are also presented. Experimental data for demagnetized samples confirm most of the theoretical results. However, the highest energy topology (doubly-charged monopoles) does not emerge in our theoretical model, while they are seen in experiments for large enough  $\gamma$ . Our results also insinuate that magnetic monopoles may be almost free in rectangular lattices with a critical ratio  $\gamma = \gamma_c = \sqrt{3}$ , supporting previous theoretical predictions.

Keywords: magnetism, spin-ice, frustration, magnetic monopoles.

Recently, the study of materials with frustrated interactions has received a lot of attention in an attempt to understand new states of matter[1–8]. The main problem concerning the experimental investigation of the properties of these structures is to find natural materials (in two and three dimensions), which not only clearly exhibit frustration but also provide reproducible results and adequate control for measurements. It is not such a simple task. An alternative path was provided by techniques of nanotechnology, in which artificial materials can be built with desirable properties and attributes in order to permit the materialization of a large variety of different sorts of geometrical frustration[9, 10]. Especially, artificial spin ices in several different lattice geometries are important examples [5, 7, 11]. They are two-dimensional (2d) arrays of elongated magnetic nanoislands, each containing an effective magnetic moment or spin (see Fig.1) that mimics natural three-dimensional (3d) spin ice materials[1–3]. However, such an artificial system in a 2d square lattice is not completely frustrated since the ice rule (in which two-spins must point-in and the other two must point-out in each vertex) is not degenerate (the two topologies that obey the ice rule have different energies[5, 6]) and, therefore, the ice regime is not stabilized. Despite this, as in natural spin ices, artificial square ice (and even other kinds of artificial lattices) also supports quasiparticle excitations that are similar to magnetic monopoles[6, 11–14], although, in general, these monopoles are of different types in natural and artificial materials. Indeed, 2d artificial square spin ice supports excitations in which

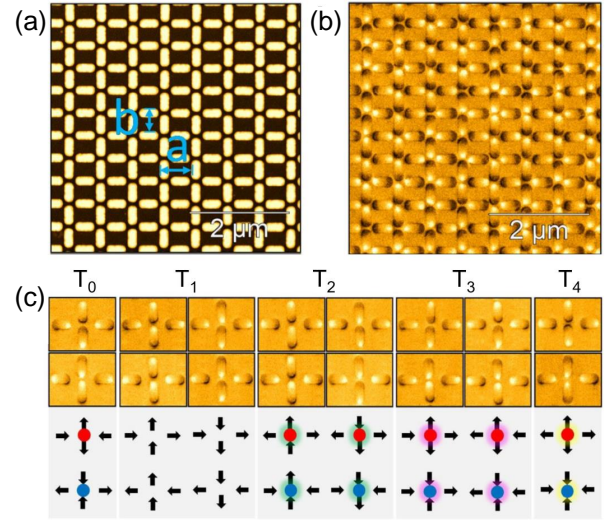


FIG. 1. Artificial spin ice in a rectangular lattice. Consistent with other types of geometry (square, kagome etc), the ground state of a rectangular spin ice obeys the ice rule in all vertices, which dictates that two spins must point-in and the other two must point-out. Excited states violate of the ice rule. The particular array shown here has the aspect ratio  $\gamma = a/b = \sqrt{2}$ , which means that the ground state should exhibit residual charges in all vertices. (a) Atomic force microscope topography of a typical sample for  $\gamma = \sqrt{2}$ . (b) Picture from the magnetic force microscope of single domain permalloy magnetic nanoislands ( $300\text{nm} \times 100\text{nm} \times 20\text{nm}$ ). Bright and dark ends of each elongated nanoisland indicate the opposite poles and give the direction of the magnetic moment of the islands and (c) The five possible topologies in this system.

\* dearaujo@ufv.br

† apereira@ufv.br.

the oppositely charged monopoles occur connected by ob-

servable and energetic strings (a kind of Nambu monopole-antimonopole pair[13, 15, 16] in contrast to Dirac monopoles, in which the string is not observable and does not have energy). Therefore, it would be interesting to imagine and construct  $2d$  artificial lattices whose monopole pair excitations would have a string tension that tends to vanish in such a way that, opposite magnetic charges would be effectively interacting only by means of the usual Coulombic law.

A recent theoretical proposal was made to modify the square array into a rectangular one [14]. Really, such a deformation can tune the ratios of the interactions between neighboring elements resulting in different magnetic ordering of the system. Denoting the horizontal and vertical lattice spacings of the rectangular array by  $a$  and  $b$  respectively, and defining a parameter (the aspect ratio) that controls the stretching of the lattice  $\gamma \equiv a/b$ , then, the ground state suffers a transition at  $\gamma = \sqrt{3}$  (or equivalently at  $1/\sqrt{3}$  by interchanging  $x$  and  $y$  axes, or make  $\gamma \geq 1$  to avoid this ambiguity). The theoretical calculations indicate that, for  $1 < \gamma < \sqrt{3}$ , the ground state (denoted *GSQ*) has residual magnetic charges (but not magnetic moments) in all vertices, alternating from positive to negative in neighboring vertices. Therefore, the total magnetic charge is zero. On the other hand, for  $\gamma > \sqrt{3}$ , the ground state (denoted *GSM*) exhibits alternating residual magnetic moments (but not charges) in all vertices and, again, in this case, the total magnetic moment is zero. Exactly at the critical value  $\gamma = \gamma_c = \sqrt{3}$ , the two different configurations *GSQ* and *GSM* have the same energy and, therefore, the ground state at this particular  $\gamma_c$  becomes degenerate, suggesting a residual entropy at absolute zero temperature similar to what happens in natural[1, 2] and (3d) artificial[8, 13, 17] spin ice materials. As a consequence, at  $\gamma_c = \sqrt{3}$  (or  $1/\sqrt{3}$ ), the string tension connecting opposite magnetic charges tends to vanish and, in principle, the monopoles become free to move. This transition of the ground state is a consequence of the fact that, differently from the square lattice (which has four distinct topologies[5] for the four spins meeting at each vertex), the rectangular lattice exhibits five topologies[14]:  $T_0, T_1, T_2, T_3, T_4$  (see Fig. 1c). The first two ( $T_0$  and  $T_1$ ) obey the ice rule (two-in, two-out) with their energies depending on the parameter  $\gamma$ . For  $1 < \gamma < \sqrt{3}$ , the energy of  $T_0$  is smaller than the energy of  $T_1$ , while the contrary is valid for  $\gamma > \sqrt{3}$ . In this letter we propose to realize an experimental study of the ground state and excited states of rectangular lattices with different ratios  $\gamma$ . Basically, we compare arrays with ratios  $\gamma < \sqrt{3}$  and  $\gamma > \sqrt{3}$  to the array having the critical value  $\gamma = \gamma_c = \sqrt{3}$  (from now, dubbed  $\gamma_c$ -array). For this comparison, we choose systems with lattices parameters having ratios equal to  $\gamma = \sqrt{2}$  and  $\gamma = \sqrt{4} = 2$ .

For the fabrication of Permalloy nanoislands, a multilayer with composition  $Si/Ta\ 3nm/Ni_{80}Fe_{20}\ 20nm/Ta\ 3nm$  was previously prepared by sputtering from tantalum (seed and cap layer) and alloyed permalloy target, on silicon oxide substrate. Then, the samples were covered with a  $85nm$  layer of  $AR - N7520.18$  negative tone photoresist and patterned by electron lithography at  $100kV$  of acceleration voltage. After development, the samples were etched by ion milling at  $20^\circ$  from normal incidence, using secondary ion mass spec-

troscopy to detect the end of the process. An ashing in oxygen plasma was subsequently performed to remove the photoresist. The nanoislands dimensions of  $l = 300nm$  and  $w = 100nm$  leads to saturation magnetization  $780 \times 10^3 Am^{-1}$ , giving a magnetic moment  $\mu = 4.68 \times 10^{-16} Am^2$  per island. Then, for the y-axis lattice spacing  $b = 450nm$  in our samples, the energy scale is  $D = \mu_0 \mu^2 / 4\pi b^3 = 2.4 \times 10^{-19} J$ . The x-axis lattice constant  $a$  ranged from  $636 - 900nm$  in such a way that we have investigated by magnetic force microscopy (*MFM*), *RASI* arrangements with aspect ratios  $a/b = \sqrt{2}, \sqrt{3}$  and  $\sqrt{4}$  (see Fig. 2). These systems were built on a area of  $4mm^2$  and the *MFM* measurements performed in  $25$  and  $100\mu m^2$  area, which enabled topologies density analysis in arrays of up  $12 \times 22$  unit cell ( $528$  islands). To improve the statistics, the *MFM* measurements were carried out in four different regions of the samples. We have also done some Monte Carlo numerical calculations of low energy configurations to compare with experimental results.

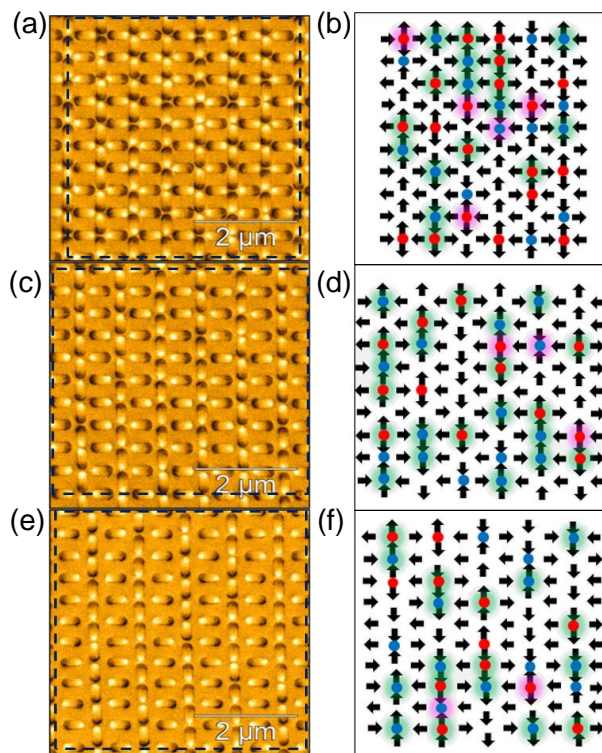


FIG. 2. *MFM* results of artificial spin ice in a rectangular lattice and representations of magnetic charges observed in each vertex with: a) and b)  $\gamma = \sqrt{2}$ ; c) and d)  $\gamma = \sqrt{3}$ ; e) and f)  $\gamma = \sqrt{4}$ .

To find low energy configurations of the nanoisland dipoles, an experimental demagnetization protocol was carried out with a commercial demagnetizer. In this process, the magnetic field is switched from positive to negative magnetic fields in sample plane at a frequency of  $60Hz$ , as the samples are moved away from the coil center. We meant to move the samples in a direction parallel to  $a$ , however due to the microstructure size of the samples, some misalignment can be expected. To optimize this procedure, we have tested two different demagnetization protocols[18]. In the first, the sample

is subjected to a sinusoidal magnetic field modulated by an exponential decay  $h(t) = H_{max} \exp(-t) \cos(2\pi 60t)$ , where  $H_{max}$  represents the field to saturate the sample. In the second, the magnetic field strength was stepped down ( $H_{max} - 0$ ) in magnitude and switched in polarity with each step. However no substantial difference was found between the two protocols; so we adopted the first one to perform the experiments.

In the simulations we have considered each magnetic nanoisland as a macro Ising spin. These spins interact via dipolar interactions. To obtain the evolution of the Ising spins under an external magnetic field, we have adopted the same procedure employed by Budrikis *et al.*[19]. In this consideration, one spin  $\hat{S}^i$  can be flipped if the total field acting on it satisfies  $(\vec{h}_{ext} + \vec{h}_{dip}^i) \cdot \hat{S}^i < -h_c^i$ , where  $\hat{S}^i$  represents a unit vector along the spin direction,  $\vec{h}_{ext}$  is the external field,  $\vec{h}_{dip}^i$  is the dipolar magnetic field produced by all spins of the lattice at the position where spin  $i$  is placed and  $h_c^i$  is the island's switching barrier. A perfect system is represented by a constant barrier while disorder can be implemented by taking  $h_c^i$  from a Gaussian distribution with standard deviation  $\sigma$ . Here we consider disorder in the system to be absorbed into the dispersion of the switching barrier.

Using the samples, we analyzed the distribution of topologies and the total magnetization for three demagnetized *RASI* arrays studied here ( $a/b = \sqrt{2}, \sqrt{3}$  and  $\sqrt{4}$ ). To accomplish that, we computationally mapped the dipole configurations imaged by *MFM* and assigned a value  $m_x = \pm 1$  or  $m_y = \pm 1$  to each island moment, depending on the island magnetic orientation, as presented in Fig.3a. The Table I summarizes the averaged experimental results, obtained after analysis. There is a very low total magnetization (in a range 0.03 – 0.10, close to zero), indicating a rather efficient demagnetization. Additionally, the experimental data for the topology densities are very different from those expected for arrays with randomly oriented individual moments ( $n(T_0) = n(T_4) = 12.5\%$ ) and ( $n(T_1) = n(T_2) = n(T_3) = 25\%$ ); this also indicates that the demagnetization protocol was successfully applied on the samples. Curiously, a few number of  $T_4$  topologies emerge for large enough  $\gamma$ , i.e., for  $\sqrt{3}$  and  $\sqrt{4}$  *RASI*. It is not seen for  $\gamma = \sqrt{2}$ . The direct experimental observation of this topology has never been predicted by our Monte Carlo calculations presented below. In terms of real lattices and nanoislands, one possible reason to explain the appearance of  $T_4$  topology in experiments (but not in simulations) is the significant reduction of the energy scale between higher and lower energy of topologies (Fig.1c).

For the ground state topologies ( $T_0$  and  $T_1$ ), we found that  $T_1$  topology as a function of  $\gamma$  has a minimum at  $\gamma = \gamma_c = \sqrt{3}$ . The same can be said for the density of the  $T_0$  topology (but with values about four times smaller than the  $T_1$  topology). On the other hand, by taking into account the presence of monopole-antimonopole pairs in these systems (excitations above the ground state associated with  $T_2$  and  $T_3$  topologies), we notice that the pair density (the sum of  $T_2$  and  $T_3$  densities) is greater for rectangular lattices with the critical aspect ratio ( $\gamma = \gamma_c$ ) than that observed for others values of  $\gamma$ . Table I summarizes these results, also indicating that critical

TABLE I. Summary of the experimental results for magnetization and topologies density for  $a/b = \sqrt{2}, \sqrt{3}$  and  $\sqrt{4}$ .

$a/b$	T0	T1	T2	T3	T4
$\sqrt{2}$	0.16911	0.45456	0.25472	0.11731	0.00430
$\sqrt{3}$	0.09050	0.40643	0.38662	0.10651	0.00994
$\sqrt{4}$	0.12656	0.43257	0.35819	0.08020	0.00248

$\gamma_c$ -arrays exhibit the maximum number of monopoles possible (i.e., the pair density and the ground state topologies as a function of  $\gamma$  would present a peak and a minimum, respectively, at  $\gamma = \gamma_c$ ). Therefore, as expected, minimum values of the ground state topologies are correlated with a maximum presence of excited states (monopole topologies).

The experimental observations were taken at room temperature (however, it is not important since these permalloy arrangements are expected to be athermal). This suggests that the different numbers of monopole pairs observed for different values of  $\gamma$  results from a purely geometrical effect, reinforcing the fact that monopoles could be more spontaneously generated in  $\gamma_c$ -arrays. Considering that the total energy of a pair depends also on the energy of the string connecting the monopole with its antimonopole, then, a reasonable hypothesis for this geometrical influence on monopole number is that the string energy decreases as  $\gamma \rightarrow \gamma_c$ , corroborating previous theoretical results[14], which predict very low string tension for  $\gamma_c$ -arrays. Indeed, in Fig. 3b, in a large section of a sample with  $\gamma = \gamma_c$ , one can observe a great quantity of monopole-antimonopole pairs (most of them with sizes  $a$  or  $b$ ) and a small quantity of isolated monopoles. We also carried out Monte Carlo (*MC*) calculations using macro Ising spins for the island dipoles to compare with experiments. To be closer to the experimental situation described above, a demagnetization field is included in the simulations. This differs from the earlier calculations[14], which do not consider external fields. Figure 4 shows the topology densities after having applied the demagnetization procedure in the *MC* simulations and its comparison with the topology densities measured by *MFM*. We can see that the final topologies depend significantly on  $\alpha$ , which is the angle that the external magnetic field is applied in relation to the larger lattice spacing (horizontal or  $a$ -axis in Fig.2). For  $\alpha < 0.15\pi$  ( $\alpha > 0.35\pi$ ) the energetic flow occurs only on horizontal (vertical) dipoles. Of course, such behavior is a consequence of the fact that, if the external field is too oblique in relation to the horizontal dipoles, the projection of this field along the perpendicular dipoles will not be sufficient to overcome the islands' switching barriers  $h_c^i$ , so the perpendicular dipoles will be frozen, i.e., they will maintain the initial configuration. We should notice that the *MC* simulations do not include the effects of thermal fluctuations, which might explain why the  $T_4$  topology is not reproduced by them. Perhaps even minor thermally induced fluctuations would be enough to help to produce the doubly-charged poles.

Initially, samples are magnetized in a diagonal direction, which implies that the topology densities are initialized to the values  $n(T_1) = 1$  and  $n(T_0) = n(T_2) = n(T_3) = n(T_4) = 0$ .

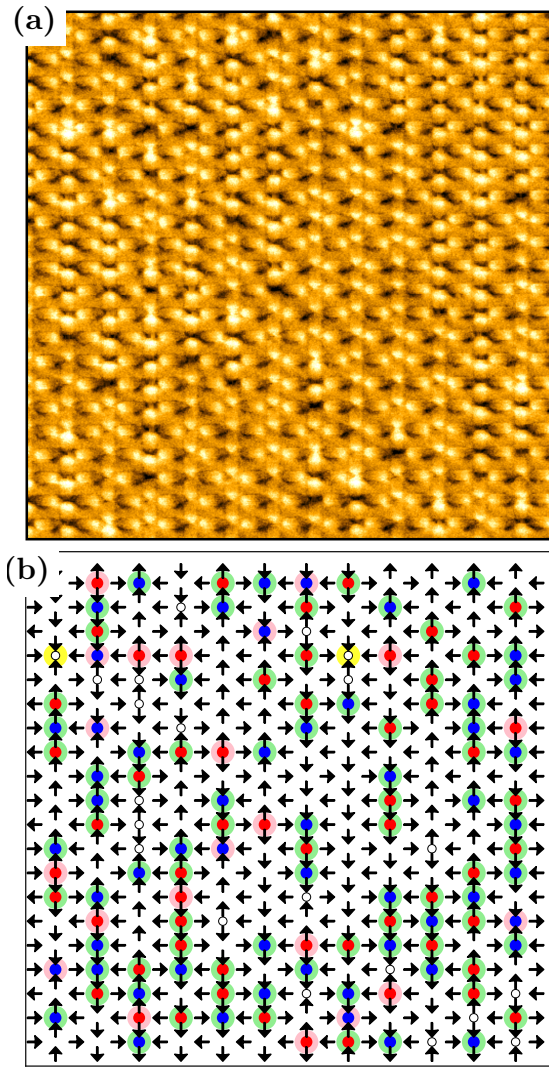


FIG. 3. (a) Large area ( $100\mu\text{m}^2$ ) MFM view of a  $\gamma = \gamma_c = \sqrt{3}$  sample and (b) magnetic moments and the topologies in each vertex, mapped computationally.

However, for  $0.25\pi < \alpha < 0.35\pi$ , the energetic flow is distributed for all the system. In Fig.4a we note that the experimental data are more similar to the theoretical results for  $\alpha \approx 0.2\pi$ , although, even for this case, our simulations were not able to exhibit the  $T_4$  topology and yet, the density of the  $T_3$  topology is also very small, arising only for large enough  $\alpha$ . Therefore, the highest topologies are responsible for the biggest contrast between theory and experiments. Maybe the system sizes used in our calculations are too small to get good statistics for the topologies of low probabilities. Figure 4b shows the experimental and theoretical behavior of topology densities for a range of lattice spacings and fixed  $\alpha = 0.20\pi$ . In overall, the theoretical results for the ground state topologies ( $T_0$  and  $T_1$ ) are in good qualitative and quantitative agreement with experimental data. However, theoretically, the  $T_0$  density goes slowly from approximately 0.20 for  $\gamma = \sqrt{2}$  to almost zero (for  $\sqrt{4}$ ), while experimentally (Table I and

Fig.4b), this density varies from 0.16 for  $\gamma = \sqrt{2}$ , decreasing to 0.09 for  $\gamma = \sqrt{3}$  (similar to theoretical results) but, it turns to increase again to 0.12 for  $\gamma = \sqrt{4}$ . Therefore, there is an important qualitative difference between our simulations and experiments in the region  $\gamma > \sqrt{3}$ . For the density of the  $T_1$  topology (green line), the MC simulations indicate that it becomes practically constant (around 0.60) as  $\gamma$  varies, while experimental data (see again the Table I) remains almost constant with  $[n(T_1)]$  varying near above 0.4. Furthermore, considering the monopole excitations ( $T_2$  and  $T_3$  topologies), we observe a good quantitative agreement between the MC simulations and experiments (Fig.4b and Table I) only for  $T_2$ -type monopole (red line). For  $T_3$  topology (cyan line), the simulations lead to a very low density as compared to experiments. Despite the differences pointed out here, we can say that, in general, there is an overall qualitative (and even quantitative) agreement between the simple Ising spin model for magnetic nanodisks used here and our experimental data. These agreements become better in the region  $1 < \gamma < \sqrt{3}$ . Finally, we have also calculated the energy of the topologies as a function of  $\gamma$  (see Fig.4c). They indicate that, independently of  $\gamma$ , the energy for creating  $T_3$  monopoles is bigger than the energy for creating  $T_2$  monopoles. It may explain the lower presence of  $T_3$  excitations around the lattice in both theoretical and experimental results. In addition, the energy of doubly-charged monopoles ( $T_4$  topology) is the biggest one, but it decreases relatively rapidly as  $\gamma$  increases. Such behavior, to some extent, justifies the direct observation of these  $T_4$  excitations in experiments for  $\gamma$  large enough ( $\gamma = \sqrt{3}$  and  $\sqrt{4}$ , see Table I).

In summary we have experimentally and theoretically investigated two-dimensional artificial spin ices in rectangular lattices. Due to the possible misalignments during the experimental demagnetization protocol, we have performed our theoretical demagnetization scheme by using an external magnetic field switched along a direction at different angles  $\alpha$  in relation to the larger cell side. The topology densities of the experimental samples (numerically counted from the MFM measurements realized in samples with  $a/b = \sqrt{2}, \sqrt{3}, \sqrt{4}$ ) were compared to the topology densities obtained theoretically by deadened sinusoidal external fields. The overall qualitative agreement between the simple theoretical model and experimental results is remarkable. A quantitative agreement is better achieved mainly when the magnetic field is applied at an angle close to  $\alpha = 0.20\pi$  in relation to the larger cell side. Therefore, in general, we can say that the experimental results confirm the simple theory of Ising spin islands most used nowadays, but interestingly, topology  $T_4$  (doubly-charged monopole), which has the highest energy, could be seen only in experiments for lattices with large enough  $\gamma$ . Concerning this fact, MC simulations are able to give, at least, a route for this experimental visualization, showing that the energy of the  $T_4$  topology decreases considerably as  $\gamma$  increases. Of course, some disagreements between the theory developed here and experiments are to be expected in view of the exceedingly complex samples as compared to the simple theoretical approach. Our results also provide experimental evidence that magnetic monopoles may be almost free in rect-

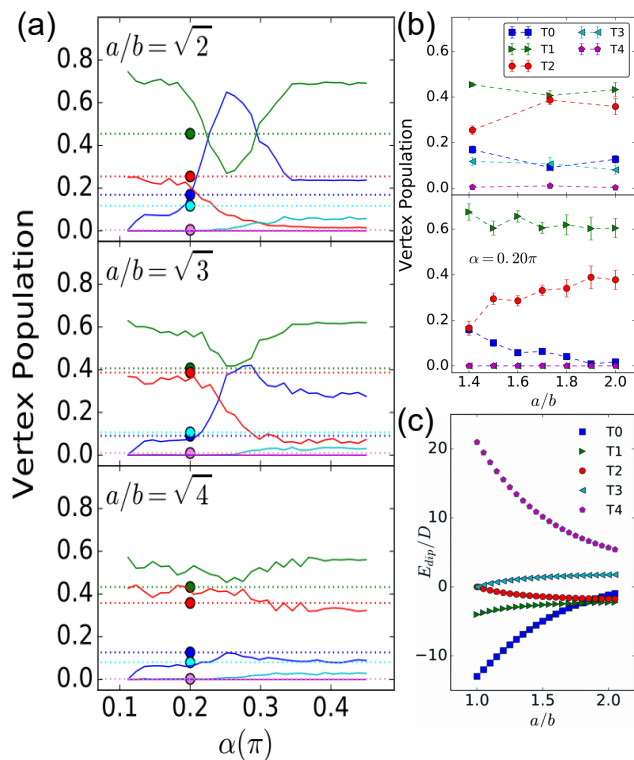


FIG. 4. (a) Vertex population densities as functions of angle  $\alpha$  between the demagnetizing field and the unitary cell along the  $x$ -axis for: (Top to bottom),  $\gamma = \sqrt{2}$ ,  $\gamma = \sqrt{3}$  and  $\gamma = \sqrt{4}$ . The colored circles represent the experimental data for  $\alpha = 0.2\pi$ . (b) Vertex population densities as functions of  $\gamma$  for the demagnetizing field fixed at  $\alpha = 0.2\pi$ . (c) Topology energies as functions of  $\gamma$ .

angular lattices at the critical aspect ratio. Indeed, the density of magnetic monopoles (topologies  $T_2$  and  $T_3$ ) is purely a geometrical effect, having a maximum at an intermediate array ( $\gamma_c$ -array). Such a phenomenon may be associated with the fact that the string tension tends to vanish as  $\gamma \rightarrow \gamma_c$ , lending support to previous theoretical predictions[14].

#### ACKNOWLEDGMENTS

The authors would like to thank the Brazilian agencies CNPq, FAPEMIG and CAPES.

- 
- [1] M. Harris, S. Bramwell, D. McMorrow, T. Zeiske, and K. Godfrey, Phys. Rev. Lett. **79**, 2554 (1997).
  - [2] C. Castelnovo, R. Moessner, and L. Sondhi, Nature **451**, 42 (2008).
  - [3] A.P. Ramirez, A. Hayashi, R.J. Cava, R. Siddharthan, and B.S. Shastry, Nature, **399**:333 (1999).
  - [4] L. Balents, Nature, **464**:199 (2010).
  - [5] R. F. Wang, C. Nisoli, R. S. Freitas, J. Li, W. McConville, B. J. Cooley, M. S. Lund, N. Samarth, C. Leighton, V. H. Crespi, and P. Schiffer, Nature **439**, 303 (2006).
  - [6] L.A. Mól, R.L. Silva, R.C. Silva, A.R. Pereira, W.A. Moura-Melo, and B.V. Costa, J. Appl. Phys. **106**, 063913 (2009).
  - [7] E. Mengotti, L.J. Heyderman, A.F. Rodriguez, F. Nolting, R.V. Hugli, and H.B. Braun, Nat. Phys. **7**, 68 (2011).
  - [8] G. Möller and R. Moessner, Phys. Rev. Lett. **96**, 237202 (2006).
  - [9] Y.-L. Wang, Z.-L. Xiao, A. Snezhko, J. Xu, L. E. Ocola, R. Divan, J. E. Pearson, G. W. Crabtree, and W.-K. Kwok, Science **352**, 962 (2016).
  - [10] C. Nisoli, V. Kapaklis, and P. Schiffer, Nat. Phys. **13**, 200 (2017).
  - [11] J.P. Morgan, A. Stein, S. Langridge, and C. Marrows, Nature Phys. **7**, 75 (2011).
  - [12] R. C. Silva, R. J. C. Lopes, L. A. S. L.A. Mól, W. A. Moura-Melo, G. M. Wysin, and A. R. Pereira, Phys. Rev. B **87**,
  - [13] L.A.S. Mól, W.A. Moura-Melo, and A.R. Pereira, Phys. Rev. B **82**, 054434 (2010).
  - [14] F.S. Nascimento, L.A.S. Mól, W.A. Moura-Melo, and A.R. Pereira, New J. Phys. **14**, 115019 (2012).
  - [15] R.C. Silva, F.S. Nascimento, L.A. S. Mól, W.A. Moura-Melo, and A.R. Pereira, New J. Phys. **14**, 015008 (2012).
  - [16] Y. Nambu, Phys. Rev. D **10**, 4262 (1974).
  - [17] G. Möller and R. Moessner, Phys. Rev. B **80**, 140409(R) (2009).
  - [18] C. Nisoli, R. Moessner, and P. Schiffer, Rev. Mod. Phys. **85**, 1473 (2013).
  - [19] Z. Budrikis, K.L. Livesey, J.P. Morgan, J. Akerman, A. Stein, S. Langridge, C.H. Marrows and R.L. Stamps, New J. Phys. **14**, 035014 (2012).